CHEMISTRY OF MATERIALS

Article

pubs.acs.org/cm

Templating C_{60} on MoS_2 Nanosheets for 2D Hybrid van der Waals *p*−*n* Nanoheterojunctions

Runfeng Chen,*[,†] Cheng Lin,[†] Huan Yu,[†] Yuting Tang,[†] Chao Song,[†] Lihui Yuwen,*[,†] Hai Li,[‡] Xiaoji Xie,*[,‡] Lianhui Wang,[†] and Wei Huang*[,‡]

[†]Key Laboratory for Organic Electronics and Information Displays & Institute of Advanced Materials, Jiangsu National Synergetic Innovation Center for Advanced Materials, Nanjing University of Posts and Telecommunications, 9 Wenyuan Road, Nanjing 210023, P. R. China

[‡]Key Laboratory of Flexible Electronics & Institute of Advanced Materials, National Synergetic Innovation Center for Advanced Materials, Nanjing Tech University, 30 South Puzhu Road, Nanjing 211816, P. R. China

Supporting Information

ABSTRACT: C_{60} and single-layer MoS_2 nanocomposites were facilely prepared via a combined solvent transfer and surface deposition (STSD) method by templating C_{60} aggregates on 2D MoS_2 nanosheets to construct hybrid van der Waals heterojunctions. The electronic property of the hybrid nanomaterials was investigated in a direct charge transport diode device configuration of ITO/C_{60}−MoS_2 nanocomposites/Al; rewritable nonvolatile resistive switching with low SET/RESET voltage (~3 V), high ON/OFF resistance ratio (~4×10^3), and superior electrical bistability (>10^4 s) of a flash memory behavior was observed. This particular electrical property of C_{60}−MoS_2 nanocomposites, not possessed by either C_{60} or MoS_2 nanosheets, was supposed to be due to the efficiently established C_{60}/MoS_2 *p*−*n* nanojunction, which controls the electron tunneling via junction barriers modulated by electric-field-induced polarization. Thus, our 2D templating method through STSD is promising to massively allocate van der Waals *p*−*n* heterojunctions in 2D nanocomposites, opening a window for important insights into the charge transport across the interface of organic/2D-semiconductors.

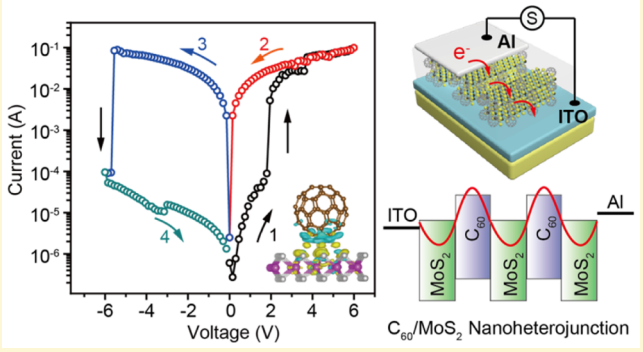

1. INTRODUCTION

Of many materials and methodologies aimed at producing low-cost and high-efficient optoelectronic devices, atomically thin-layered two-dimensional (2D) materials appear particularly promising for new-generation optoelectronic applications, owing to their intriguing electronic, optical, and mechanical properties.[1−3] As a typical 2D transition metal chalcogenide (TMD) material with strong intralayer covalent bonding but weak interlayer van der Waals interaction,[4−6] molybdenum disulfide (MoS_2) nanosheet prepared by either physical or chemical exfoliation methods exhibits excellent electrical and optical properties with unique direct bandgap features for a large number of optoelectronic applications.[7−9] Especially, the large and flat surface of MoS_2 nanoflakes can act as an efficient template to construct 2D TMD nanosheet-templated composites. A wide range of materials, including noble metals (Pd, Pt, and Ag[10,11]), inorganic semiconductors (TiO_2 and Bi_2S_3[12,13]), other 2D nanosheets (graphene, graphene oxide, hexagonal boron nitride, and WS_2[14−18]), polymers (polyvinylpyrrolidone, polyethylene glycol, and polyaniline[19,20]), and organic aggregates,[21] have been introduced onto the MoS_2 surface to achieve 2D hybrid functional materials. Materials that are free of dangling bonds and native surface oxides are known to interact via van der Waals force with the 2D nanosheets. However, a clear understanding of the charge transport or energy transfer across the composite interface is still lacking. Nevertheless, enhanced electronic, photonic, or catalytic properties of these integrated MoS_2 nanocomposites were generally evidenced with improved device performance, especially when the introduced materials were effectively assembled in nanoscale with preferred orientation and alignment on the 2D molecular surface of MoS_2 nanosheets.

Fullerenes have long been considered as promising building blocks for optoelectronic devices, benefited from their unique physical, chemical, and mechanical properties.[22,23] However, the introduction of fullerenes onto the 2D-nanosheet surface of MoS_2 to produce C_{60}−MoS_2 hybrid nanocomposites was rarely reported,[24] despite their interesting properties suggested by simulation studies.[25] The recent attempt on the experimental preparation of C_{60}−MoS_2 nanocomposite was performed by Remškar et al. in 2005 using a catalyzed transport reaction typically run at 1030 K under a pressure of 10^{-3} Pa for 22

Received: March 21, 2016
Revised: May 11, 2016
Published: May 31, 2016

DOI: 10.1021/acs.chemmater.6b01115
Chem. Mater. 2016, 28, 4300−4306

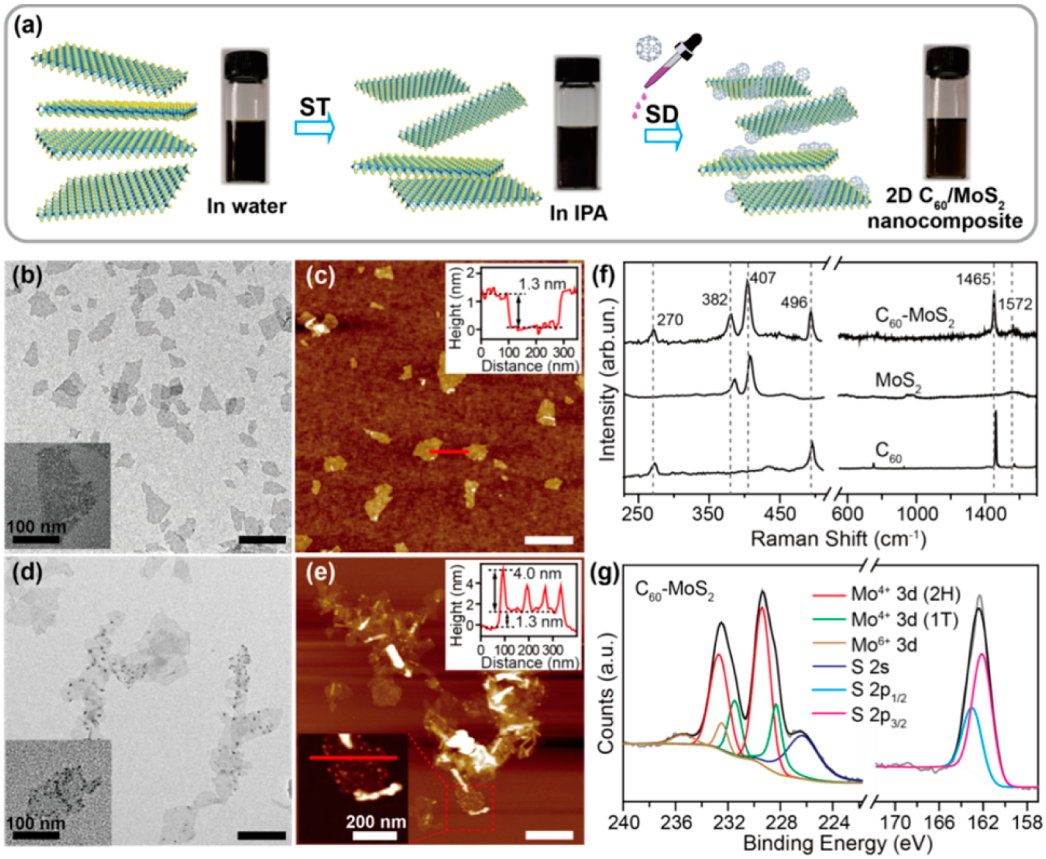

Figure 1. (a) Preparation of 2D C_{60}–MoS_2 nanocomposites through solvent transfer (ST) and surface deposition (SD) methods. (b,d) TEM and (c,e) AFM images of MoS_2 nanosheets transferred to isopropyl alcohol (b,c) and C_{60}–MoS_2 nanocomposites (d,e) with corresponding AFM height profiles (inset). (f) Raman spectra of C_{60}, MoS_2 nanosheets, and C_{60}–MoS_2 nanocomposites. (g) High-resolution XPS spectra of the C_{60}–MoS_2 nanocomposites. Scale bars are 500 nm for panels b, c, d, and e.

days.[24] This harsh preparation condition significantly hindered the experimental studies and applications of C_{60}–MoS_2 hybrid nanocomposite materials, let alone the charge transport property studies of the C_{60}/MoS_2 junctions. Here, we present a convenient yet successful and scalable method for C_{60}–MoS_2 nanocomposite preparation under ambient conditions in less than 30 min via solvent transfer and surface deposition (STSD). The charge transport across the efficiently constructed van der Waals C_{60}/MoS_2 nanoheterojunctions were investigated, for the first time, in direct charge transport diode devices. Extraordinary high-performance nonvolatile flash memory behavior was observed with low threshold voltage below 2.0 V and high ON/OFF ratio up to 3.8×10^3; these data are among the best of the reported memory devices based on MoS_2 nanomaterials (Table S1). Comprehensive experimental and computational studies reveal that C_{60} forms a type-II p–n heterojunction with MoS_2, which determines the current–voltage (I–V) characteristics of the devices. Our results presented here provide insightful guidance for the search and design of novel promising 2D nanoheterojunction-based composites with extraordinary electronic transport properties.

2. RESULTS AND DISCUSSION

2.1. Preparation and Characterization of the C_{60}–MoS_2 Nanocomposites. Due to the large solubility difference of MoS_2 and C_{60} in solvents, conventional method by mixing them in a cosolvent is hard to be realized for the preparation of C_{60}–MoS_2 nanocomposites. To solve this issue, we developed a combined solvent transfer and surface deposition (STSD) method in two steps. First, the water-dispersible MoS_2 nanosheets exfoliated chemically via ultrasonication enhanced lithium intercalation were transferred to isopropyl alcohol (IPA); IPA is miscible with toluene, which can dissolve C_{60} very well.[26] Second, to this IPA-dispersed MoS_2 nanosheets, various amount of C_{60} toluene solution (1 mg/mL) was injected slowly. Since the solubility of C_{60} in IPA is low, the gradually precipitated C_{60} will deposit preferably on the hydrophobic parts of MoS_2 nanosheet surface, resulting in a stable and well-dispersed C_{60}–MoS_2 nanocomposite in IPA (Figure 1a).

The as-prepared C_{60}–MoS_2 nanocomposites by the STSD method were characterized by a combination of transmission electron microscopy (TEM), atom force microscopy (AFM), Raman spectrum, and X-ray photoelectron spectroscopy (XPS) measurements. According to the TEM images, the Li-intercalated MoS_2 nanosheets in water have uniform morphology with size ranging from 200 to 500 nm (Figure S1a). The thickness of MoS_2 nanosheets was identified to be about 1.4 nm by the height mode of AFM (Figure S2); this thickness is identical to the value of the chemically exfoliated single-layer MoS_2.[27] When the water-dispersed MoS_2 nanosheets were transferred to IPA solution, the strongly hydrophilic parts of MoS_2 nanosheets that cannot be well dispersed in IPA were removed by centrifugation; the remaining MoS_2 nanosheets in IPA were partially hydrophobic for good dispersion in organic solvent of IPA, although they were slightly aggregated as revealed by TEM and AFM images (Figure 1b,c). Onto the 2D

DOI: 10.1021/acs.chemmater.6b01115
Chem. Mater. 2016, 28, 4300–4306

molecular surface of MoS_2 nanosheets in IPA, C_{60} molecules were deposited via surface deposition by controlling the solvent miscibility and solubility difference of C_{60} in toluene and IPA and by taking advantages of the hydrophobic feature of MoS_2 surface. The accommodated C_{60} aggregates with about 15 nm in diameter (by TEM and AFM) and 5 nm in height (by AFM) were identified to anchored randomly on the surface of the single-layer MoS_2 nanosheets to form a well-dispersed C_{60}–MoS_2 hybrid nanocomposite (Figure 1d,e). High-resolution TEM images (Figure S3a,b) show the typical hexagonal single crystal structure of MoS_2 with a distance of 0.27 nm for the (100) Mo atoms and the 6-fold selected area electron diffraction (SAED) pattern for both (100) and (110) planes.[28] After the STSD processing, the crystal structure of the chemically exfoliated MoS_2 nanosheets remains in the amorphous C_{60} aggregate-deposited C_{60}–MoS_2 nanocomposites (Figure S3c,d).

The successfully prepared single-layer MoS_2 nanosheets and the C_{60}–MoS_2 hybrid nanocomposite were further characterized by the Raman spectra. When C_{60} is deposited onto the MoS_2 nanosheets, an additional new Raman peak of C_{60} appears at 1465 cm^{-1}, which is slightly blue-shifted in comparison with that of pure C_{60};[29] the two characteristic in-plane (E^1_{2g}) and out-of-plane (A_{1g}) Raman modes of MoS_2 nanosheets[30] are also blue-shifted (Figure 1f), suggesting quite significant and strong interactions between C_{60} and MoS_2 nanosheets. This interaction maybe serve as the main driving force for the formation of the stable and abundant 2D C_{60}/MoS_2 heteronanostructures. It can be also noticed from the TEM and AFM images (Figure 1d,e) that some MoS_2 nanosheets (40%) are free of C_{60} deposition, due to the different surface states of the chemically exfoliated MoS_2 nanosheets; the hydrophobic surface of the MoS_2 nanosheets must be better for the adhesion and templating of hydrophobic C_{60} aggregates. About 60% MoS_2 nanosheets are hydrophobic enough for C_{60} coverage.

XPS was carried out to investigate the structure and composition of the resulted C_{60}–MoS_2 nanocomposites. Characteristic Mo and S peaks without significant impurities were observed (Figure S4).[31] Through careful deconvolution of the high-resolution XPS spectra, the binding energy peaks ranging from 220 to 240 eV were fitted into four groups (Figure 1g). Trigonal prismatic (2H) MoS_2 was found to have the strongest doublet peaks at 232.6 and 229.4 eV belong to Mo^{4+} $3d_{3/2}$ and Mo^{4+} $3d_{5/2}$, respectively; these Mo^{4+} 3d peaks (231.4 and 228.4 eV) at octahedral (1T) configuration are relatively weaker.[32] From the area of Mo^{4+} 3d peaks of 1T and 2H phases, we can infer that 2H is the main phase of the C_{60}–MoS_2 nanocomposites, which is identical to that of the MoS2 nanosheets before C_{60} deposition (Figure S5). A trace of higher oxidation state of Mo (Mo^{6+} 3d), which may originate from the partial oxidation of Mo atoms at the edges or defects on the crystal plane during chemical exfoliation, was also identified to have weak peaks around 235 and 232 eV. The singlet 2s peak of S atom is located at 226.2 eV, while its 2p peaks are at 163.0 and 162.1 eV. No sulfur oxidation was detected in the composites (Figure 1g).[28]

2.2. Electronic Properties of the C_{60}–MoS_2 Nanocomposites. In an effort to better understand and exploit the potential of the newly constructed C_{60}–MoS_2 nanocomposites with 2D-layer templated C_{60} molecules on the direct bandgap single-layer MoS_2, the composites were tested as active layers in direct charge transport diode devices with a configuration of ITO/C_{60}–MoS_2 (50 nm)/Al (Figures S6 and S7), where ITO and Al are the bottom and top electrodes, respectively.[33] The current–voltage (I–V) characteristics of the devices measured at room temperature and ambient atmosphere showed an extraordinary flash memory behavior (Figure 2a). When a

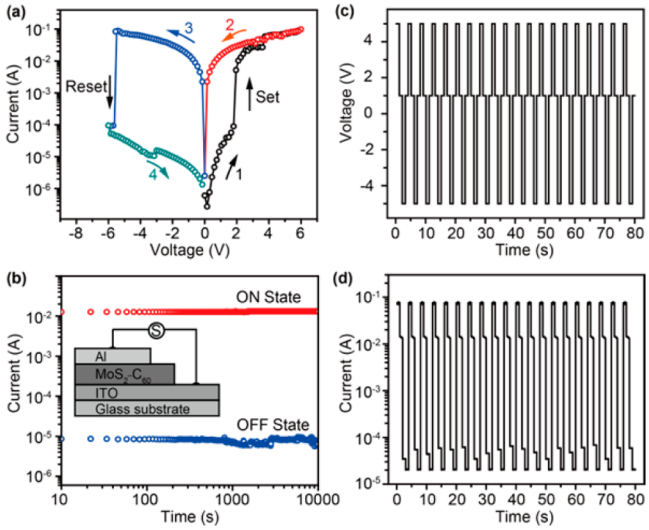

Figure 2. (a) I–V characteristics of the ITO/C60-MoS2/Al diode memory device. (b) Retention times of the ON and OFF states of the memory device probed with a voltage of 1.0 V. Inset: memory device structure. (c) Input and (d) output of write–read–erase–read (WRER) cycles of the memory device for flash storage applications. Voltages for WRER cycles are +5, 1, −5, and 1 V, respectively.

positive voltage is applied from 0 to 6 V (first sweep), the device is initially OFF with a low current density, then an abrupt current jump occurs at 2.2 V to generate ON state, which represents a "writing" process of memory devices. The high conductivity can be read in the subsequent positive sweep (second sweep) and reverse sweep (third sweep, ≥−5.5 V). Importantly, when the negative sweep voltage is lower than −5.5 V, the high-conductive ON state can be switched back to the original low-conductive OFF state, serving as "erasing" process of memory devices; the OFF state can be read (fourth sweep) and reprogrammed to the ON state in the next positive sweep, leading to a repeatable "write–read–erase–read–rewrite" cycle for a rewritable nonvolatile flash memory device.[34]

The ratios of current density on the ON state to that on the OFF state of the memory device are about 2×10^3 and 3.8×10^3 at positive and negative sweeps, respectively. Moreover, the memory device is highly stable with retention time longer than 10^4 s and a fluctuation below 10% (Figure 2b), which is favorable for the steady running of flash type memory writing–reading–erasing cycles acted on continuous voltage signals at 5 V (write), 1 V (read), −5 V (erase), and 1 V (read), respectively (Figure 2c,d). The stable and high ON/OFF current ratio of the flash memory based on C_{60}–MoS_2 nanocomposites is promising and advantageous to minimize the misreading probability for the long-term operation of memory devices.

To reveal the particular conductance switching of the flash memory, the charge transport behavior of the 2D nanocomposite under electronic fields was investigated by model-fitting of the experimental I–V data (Figure 3a). The OFF-state

DOI: 10.1021/acs.chemmater.6b01115
Chem. Mater. 2016, 28, 4300–4306

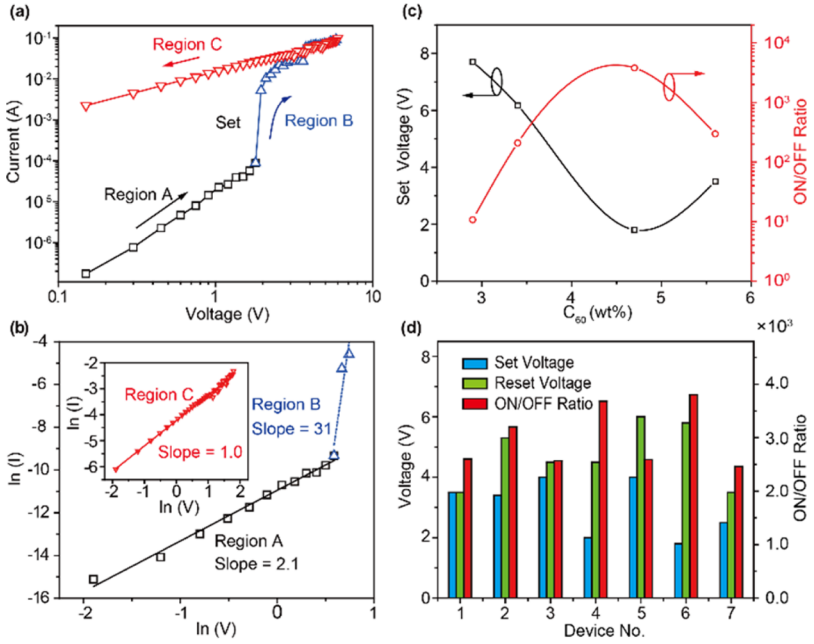

Figure 3. (a) Experimental $I-V$ characteristics of the ITO/C_{60}–MoS_2 nanocomposites/Al diode memory device under the positive voltage sweep. (b) Experimental data points and fitted lines of the $I-V$ curves in OFF state of region A and ON state of regions B and C. (c) Effect of the C_{60} weight content on the turn-on (set) voltage and ON/OFF ratio of the device. (d) The performance variations of the devices.

current density (I) can be well-fitted by the space-charge-limited current (SCLC) model (eq 1):

$$I \propto \frac{9\varepsilon_i \mu V^2}{8d^3} \tag{1}$$

where V is the applied voltage, ε_i is the dynamic dielectric constant, μ is the charge carrier mobility, and d is the film layer thickness.[19] The plot of $\ln(I)$ vs $\ln(V)$ is in a line at the OFF-state (Region A) with a slope of 2.1, suggesting a typical SCLC mechanism (Figure 3b). With the continuous increase of voltage, the current increases exponentially as $I \approx V^m$ ($m = 31$) in the switching region of Region B. In contrast, the $I-V$ curve at the ON-state (Region C) was found to be in line with the ohmic conduction model (eq 2) from the linear relationship between $\ln(I)$ and $\ln(V)$ with a slope very close to 1.0 (Figure 3b)

$$I \propto V \exp\left(\frac{-\Delta E_{ae}}{kT}\right) \tag{2}$$

where ΔE_{ae} is the activation energy of electrons, k is the Boltzmann constant, and T is the temperature.

It should be noted that both single-component C_{60} and single-layer MoS_2 nanosheets show high current density without any memory characteristics (Figure S8) at the identical device configuration and measurement conditions, which are in agreement with previous literature reports.[19] The new-emerged memory behavior of their composite, found first in this study, should be a joint effect from both sides of C_{60} and MoS_2. Consequently, the composition of the nanocomposites must be very critical. We then examined the effect of C_{60} weight content on the memory device performance. As shown in Figure 3c, when the content of C_{60} is lower than 3 wt % or higher than 6 wt %, the ON/OFF ratio will be decreased with increased SET and RESET voltages; the optimal C_{60} content is around 5 wt % for the highest ON/OFF ratio and the lowest SET and RESET voltages. At this optimal C_{60} content, we then tested the repeatability of the memory performance. From seven independently fabricated devices, the flash memory behaviors were all observed with varied ON/OFF ratios from 2.5×10^3 to 3.8×10^3, SET voltages from 1.9 to 4.0 V, and RESET voltages from 3.5 to 6.0 V (Figure 3d). The good repeatability of the high-performance flash memory based on C_{60}–MoS_2 nanocomposites gives the advantages of perfect performance control for practical applications.

2.3. Feature of C_{60}/MoS_2 Nanoheterojunction. Considering that diode devices are functioned on a composite film with a thickness of 50 nm, the layer number of MoS_2 nanosheets in the conductive channel should be more than 10, according to the sizes of C_{60}–MoS_2 nanocomposites (~5 nm thick) and nondeposited MoS_2 (1.4 nm thick). With the coverage percent of C_{60} on MoS_2 (60%), the possibility for charge transport through only MoS_2 over more than 10 stacks is very low ($<0.4^{10}$). Therefore, the charge current should pass through the C_{60}/MoS_2 nanojunction for several times during the operation of the device, resulting in the special electrical property of bipolar resistance switching behavior.

To identify the origin of the extraordinary flash memory performance of the C_{60}–MoS_2 nanocomposites due to C_{60}/MoS_2 nanojunctions, first-principal calculations were performed using the Vienna ab initio simulation package (VASP) to figure out the particular interactions between C_{60} and MoS_2. In accord with previous findings[25] that C_{60} prefers to be attached with a hexagon parallel to MoS_2 layer and charge depletes mostly from the bottom of C_{60} and accumulates at the interface as shown by the charge redistribution at the nanojuction by subtracting the electron of the hybrid system from that of the isolated components of C_{60} and MoS_2 (Figure 4), indicating the formation of C_{60}/MoS_2 $p-n$ heterojunction in type-II band alignment.[35]

The VASP calculation results are well in line with the frontier orbital analysis based on the highest occupied molecular orbital (HOMO) and the lowest unoccupied molecular orbital

DOI: 10.1021/acs.chemmater.6b01115
Chem. Mater. 2016, 28, 4300–4306

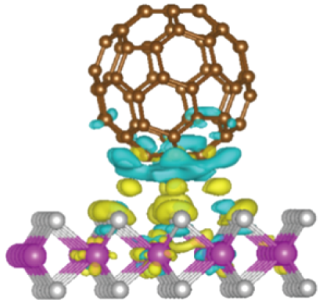

Figure 4. VASP calculated charge density differences before and after the C_{60}/MoS_2 junction formation. The yellow and cyan regions represent electron accumulation and depletion, respectively.

(LUMO) energy levels (Figure 5a). The work functions of ITO and Al electrodes are much closer to the LUMOs of MoS_2 and

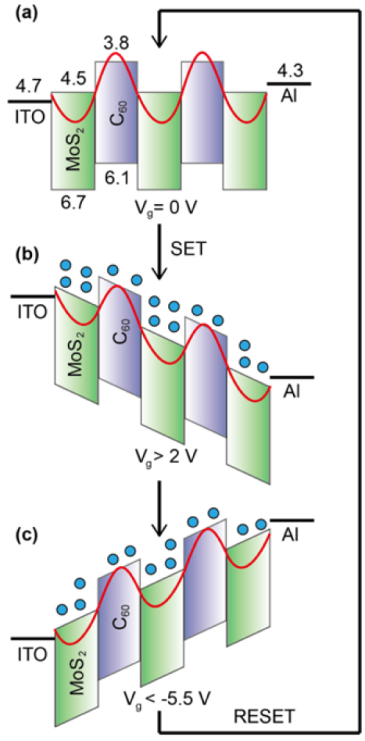

Figure 5. Charge transport mechanism across the C_{60}/MoS_2 $p-n$ nanoheterojunction: (a) Energy level diagram of the flash memory diode device at the initial state when the applied voltage (V_g) at 0 V. (b) The device is set to ON when V_g is higher than 2.0 V to induce polarization strong enough to reduce the junction barriers for high conductivity. (c) The device is reset to OFF after V_g is lower than −5.5 V to eliminate the polarization and restore the junction barriers for low conductivity. Then, the device is turned back to the initial state.

C_{60} than to their HOMO, suggesting the main charge carrier of the memory devices should be the electron that transfers between the LUMOs of the active layer molecules. The lower LUMO of MoS_2 (−4.5 eV) than that of C_{60} (−3.8 eV) leads to slightly accumulated electrons on MoS_2 when they contact in composite materials to form a nanojunction, suggesting again the formation of type-II alignment with a built-in potential to rectify the $I-V$ characteristics significantly.

2.4. Model for the Charge Transport Across the C_{60}/MoS_2 $p-n$ Nanoheterojunction. On the basis of both experimental and theoretical evidence, we can propose a possible mechanism for the flash memory behavior of this new-constructed nanocomposite system containing plenty of $p-n$ heterojunctions. Based on a model of electron tunneling across the polarization potential barriers,[36] the electron conductive can be modulated by the changing of electric-field at various driving voltages. For the well-dispersed C_{60} aggregates on MoS_2 nanosheets, the contact between the adjacent C_{60} and MoS_2 results in massive interfaces and junction barriers, which dominate the electron transport and make the diode initially at the OFF state (Figure 5a). Setting the applied electric field to a low value, the injected electrons will gradually accumulate in the MoS_2 side of the C_{60}/MoS_2 junction following the SCLC model and thus result in the formation of polarized domains. The steadily increased electron density in MoS_2 reduces the junction-barrier height, allowing facile electron tunneling and transportation to/from the conductive pathway along all the interfaces of C_{60}/MoS_2 to set the diode to the ON state (Figure 5b). Because of the existence of bound charges and internal polarization fields, the conductive pathway is stable and can survive until a reversely applied electric field is high enough to rupture the polarized domains (Figure 5c). Once the accumulated electron are relaxed to a certain level, the junction barriers of C_{60}/MoS_2 will resume the initial height, hindering the electron transportation and destroying the conductive pathway to reset the diode device to OFF state (Figure 5a).

3. CONCLUSIONS

In summary, we have developed a facile and efficient STSD method for the preparation of 2D templated $C_{60}-MoS_2$ hybrid nanocomposites with abundant van der Waals $p-n$ nano-heterojunctions; the obtained C_{60}/MoS_2 composites, showing extraordinary properties that are not hold by either C_{60} or MoS_2, was exploited as an active layer in conventional diode memory devices to investigate the charge transport properties of the $p-n$ nanoheterojunctions. The devices exhibit sustainable conductivity bistability and typical bipolar resistance switching phenomenon with low SET (1.9 V) and RESET (−5.5 V) voltages and high ON/OFF resistance ratio (~4×10^3). A model of the electron tunneling across the junction barriers modulated by electric-field-induced polarization was proposed to be the main mechanism for the observed flash memory behavior of the $C_{60}-MoS_2$ composites, providing important insights into the particular charge transport and transfer behaviors across the interface between the organic and 2D semiconductors in a type-II band alignment for the first time. With the availability of a large library of organic molecules and ultrathin 2D TMDs, the technique presented here can likely be scaled up to achieve high-performance organic/2D semiconductor van der Waals heteronanostructures for use in a wide range of optoelectronic applications.

4. EXPERIMENTAL SECTION

4.1. Preparation of $C_{60}-MoS_2$ Hybrid Nanocomposites. Single-layer molybdenum disulfide (MoS_2) nanosheets were prepared according to ultrasonication enhanced lithium intercalation method reported recently.[27,37,38] The aqueous MoS_2 solution (2.0 mg/mL, 3 mL) was centrifuged and transferred to isopropyl alcohol (IPA) solution (1.0 mg/mL) for the composites preparation. The $C_{60}-MoS_2$ hybrid nanosheets with various weight content of C_{60} from 2.9%, 3.4%, 4.7%, and 5.6% were prepared by injecting various amount of C_{60} toluene solution (2 mg/mL) slowly to the isopropyl alcohol solution of MoS_2, accompanied by ultrasonication for 20 min at room temperature.

DOI: 10.1021/acs.chemmater.6b01115
Chem. Mater. 2016, 28, 4300−4306

4.2. Characterization and Calculation. The AFM images were obtained by using Bruker Dimension Icon in tapping mode. The Raman spectra were recorded on a WITec CRM200 confocal Raman microscopy system using a 488 nm laser with an air cooling charge coupled device (CCD) as detector. TEM measurements were performed on a JEM2100 transmission electron microscope with an accelerating voltage of 200 kV. High resolution TEM (HRTEM) characterization was performed using a Tecnai G2 F20 S-Twin delectron microscope. XPS spectra of the C_{60}−MoS_2 nanocomposites were measured using a PHI 5000 VersaProbe with Al K_α as the excitation source and calibrated using the C 1s peak at 284.6 eV as a reference. The optical microscope and scanning electron microscopy (SEM) images of the diode device were obtained by Olympus BX43 and Hitachi S-4800, respectively.

4.3. Fabrication and Characterization of Diode Devices. The patterned indium tin oxide (ITO) glass substrates were cleaned in a standard procedure for spin-coating an active layer of C_{60}−MoS_2 hybrid nanocomposites from 1.0 mg/mL solution, followed by annealing at 120 °C for 15 min to remove residual solvents. The thickness of the composite film measured by a spectroscopic ellipsometry (α-SE, J. A. Wollam Co. Inc.) was adjusted to 50 nm by controlling the spin-coating conditions. Then, Al was thermally evaporated onto the film surface at 5×10^{-4} Pa through a shadow mask to yield top Al electrodes with active area of 0.4×0.4 mm^2. The devices without encapsulation were measured immediately under ambient atmosphere conditions. The current−voltage (I−V) characteristics of the devices were recorded by a Keithley 2400 source-meter.

■ ASSOCIATED CONTENT

Supporting Information

The Supporting Information is available free of charge on the ACS Publications website at DOI: 10.1021/acs.chemmater.6b01115.

Detailed preparation, characterization, and calculation of C_{60}−MoS_2hybrid nanosheets; fabrications and measurements of the diode devices (PDF)

■ AUTHOR INFORMATION

Corresponding Authors

*E-mail: iamrfchen@njupt.edu.cn.
*E-mail: iamlhyuwen@njupt.edu.cn.
*E-mail: iamxjxie@njtech.edu.cn.
*E-mail: wei-huang@njtech.edu.cn.

Author Contributions

The manuscript was written through contributions of all authors. All authors have given approval to the final version of the manuscript.

Notes

The authors declare no competing financial interest.

■ ACKNOWLEDGMENTS

This study was supported in part by the National Natural Science Foundation of China (21274065, 21304049, 21001065, and 61136003), Qing Lan project of Jiangsu province, and Science Fund for Distinguished Young Scholars of Jiangsu Province of China (BK20150041).

■ REFERENCES

(1) Chhowalla, M.; Shin, H. S.; Eda, G.; Li, L.; Loh, K. P.; Zhang, H. The Chemistry of Two-Dimensional Layered Transition Metal Dichalcogenide Nanosheets. *Nat. Chem.* **2013**, *5*, 263−275.

(2) Wang, Q. H.; Kalantar-Zadeh, K.; Kis, A. J.; Coleman, N.; Strano, M. S. Electronics and Optoelectronics of Two-Dimensional Transition Metal Dichalcogenides. *Nat. Nanotechnol.* **2012**, *7*, 699−712.

(3) Kim, C.; Nguyen, T. P.; Le, Q. V.; Jeon, J.; Jang, H. W.; Kim, S. Y. Performances of Liquid-Exfoliated Transition Metal Dichalcogenides as Hole Injection Layers in Organic Light-Emitting Diodes. *Adv. Funct. Mater.* **2015**, *25*, 4512−4519.

(4) Liu, J.; Yin, Z.; Cao, X.; Zhao, F.; Lin, A.; Xie, L.; Fan, Q.; Boey, F.; Zhang, H.; Huang, W. Bulk Heterojunction Polymer Memory Devices with Reduced Graphene Oxide as Electrodes. *ACS Nano* **2010**, *4*, 3987−3992.

(5) Geim, A. K.; Grigorieva, I. V. Van der Waals Heterostructures. *Nature* **2013**, *499*, 419−425.

(6) Cui, X.; Lee, G.; Kim, Y. D.; Arefe, G.; Huang, P. Y.; Lee, C.; Chenet, D. A.; Zhang, X.; Wang, L.; Ye, F.; Pizzocchero, F.; Jessen, B. S.; Watanabe, K.; Taniguchi, T.; Muller, D. A.; Low, T.; Kim, P.; Hone, J. Multi-terminal Transport Measurements of MoS_2 using a van der Waals Heterostructure Device Platform. *Nat. Nanotechnol.* **2015**, *10*, 534−540.

(7) Gao, P.; Wang, L.; Zhang, Y.; Huang, Y.; Liu, K. Atomic-Scale Probing the Dynamics of Sodium Transport and Intercalation Induced Phase Transformations in MoS_2. *ACS Nano* **2015**, *9*, 11296−11301.

(8) Bertolazzi, S.; Krasnozhon, D.; Kis, A. Nonvolatile Memory Cells Based on MoS_2/Graphene Heterostructures. *ACS Nano* **2013**, *7*, 3246−3252.

(9) Tang, P.; Xiao, J. J.; Zheng, C.; Wang, S.; Chen, R. F. Graphene-Like Molybdenum Disulfide and Its Application in Optoelectronic Devices. *Acta. Phys-Chim. Sin.* **2013**, *29*, 667−677.

(10) Huang, X.; Zeng, Z.; Bao, S.; Wang, M.; Qi, X.; Fan, Z.; Zhang, H. Solution-Phase Epitaxial Growth of Noble Metal Nanostructures on Dispersible Single-Layer Molybdenum Disulfide Nanosheets. *Nat. Commun.* **2013**, *4*, 1444.

(11) Wang, X.; Meng, G.; Zhu, C.; Huang, Z.; Qian, Y.; Sun, K.; Zhu, X. A Generic Synthetic Approach to Large-Scale Pristine-Graphene/Metal-Nanoparticles Hybrids. *Adv. Funct. Mater.* **2013**, *23*, 5771−5777.

(12) Li, J.; Ma, H.; Wu, D.; Li, X.; Zhao, Y.; Zhang, Y.; Du, B.; Wei, Q. A label-free electrochemiluminescence immunosensor based on $KNbO_3$−Au Nanoparticles@Bi_2S_3 for the Detection of Prostate Specific Antigen. *Biosens. Bioelectron.* **2015**, *74*, 104−112.

(13) Huang, X.; Qi, X. Y.; Boey, F.; Zhang, H. Graphene-based Composites. *Chem. Soc. Rev.* **2012**, *41*, 666−686.

(14) Yin, Z.; Zeng, Z.; Liu, J.; He, Q.; Chen, P.; Zhang, H. Memory Devices Using a Mixture of MoS_2 and Graphene Oxide as the Active Layer. *Small* **2013**, *9*, 727−731.

(15) Shinde, S. M.; Kalita, G.; Tanemura, M. Fabrication of poly(methyl methacrylate)-MoS_2/graphene Heterostructure for Memory Device Application. *J. Appl. Phys.* **2014**, *116*, 214306.

(16) Wang, J.; Wang, Z.; Cho, H.; Kim, M. J.; Sham, T. K.; Sun, X. Layer Speciation and Electronic Structure Investigation of Free-standing Hexagonal Boron Nitride Nanosheets. *Nanoscale* **2015**, *7*, 1718−1724.

(17) Hong, X.; Kim, J.; Shi, S.; Zhang, Y.; Jin, C.; Sun, Y.; Tongay, S.; Wu, J.; Zhang, Y.; Wang, F. Ultrafast Charge Transfer in Atomically Thin MoS_2/WS_2 Heterostructures. *Nat. Nanotechnol.* **2014**, *9*, 682−686.

(18) Coleman, J. N.; Lotya, M.; O'Neill, A.; Bergin, S. D.; King, P. J.; Khan, U.; Young, K.; Gaucher, A.; De, S.; Smith, R. J.; Shvets, I. V.; Arora, S. K.; Stanton, G.; Kim, H.; Lee, K.; Kim, G. T.; Duesberg, G. S.; Hallam, T.; Boland, J. J.; Wang, J. J.; Donegan, J. F.; Grunlan, J. C.; Moriarty, G.; Shmeliov, A.; Nicholls, R. J.; Perkins, J. M.; Grieveson, E. M.; Theuwissen, K.; McComb, D. W.; Nellist, P. D.; Nicolosi, V. Two-Dimensional Nanosheets Produced by Liquid Exfoliation of Layered Materials. *Science* **2011**, *331*, 568−571.

(19) Liu, J.; Zeng, Z.; Cao, X.; Lu, G.; Wang, L.; Fan, Q.; Huang, W.; Zhang, H. Preparation of MoS_2 -Polyvinylpyrrolidone Nanocomposites for Flexible Nonvolatile Rewritable Memory Devices with Reduced Graphene Oxide Electrodes. *Small* **2012**, *8*, 3517−3522.

(20) Pereiraa, V. R.; Isloor, A. M.; Ahmedb, A. A.; Ismail, A. F. Preparation, Characterization and the Effect of PANI Coated TiO_2 Nanocomposites on The Performance of Polysulfone Ultrafiltration Membranes. *New J. Chem.* **2015**, *39*, 703−712.

DOI: 10.1021/acs.chemmater.6b01115
Chem. Mater. 2016, 28, 4300−4306

(21) Tan, C.; Qi, X.; Huang, X.; Yang, J.; Zheng, B.; An, Z.; Chen, R.; Wei, J.; Tang, B. Z.; Huang, W.; Zhang, H. Single-Layer Transition Metal Dichalcogenide Nanosheet-Assisted Assembly of Aggregation-Induced Emission Molecules to Form Organic Nanosheets with Enhanced Fluorescence. *Adv. Mater.* **2014**, *26*, 1735−1739.
(22) Seol, J.; Monroe, M. L.; Anderson, T. J.; Hasnain, M. A.; Park, C. Effect of ITO Surface Treatment On Organic Solar Cells. *IEEE* **2006**, 236−239.
(23) Kwong, C. Y.; Chui, P. C. Indium−tin−oxide surface treatments: Influence on the Performance of CuPc/C_{60} Solar Cells. *J. Appl. Phys.* **2003**, *9*, 5472−5479.
(24) Remškar, M.; Mrzel, A.; Jesih, A.; Kovač, J.; Cohen, H.; Sanjines, R.; Levy, F. New Composite MoS_2-C_{60} Crystals. *Adv. Mater.* **2005**, *17*, 911−914.
(25) Gan, L.; Zhang, Q.; Cheng, Y.; Schwingenschlögl, U. Photovoltaic Heterojunctions of Fullerenes with MoS_2 and WS_2 Monolayers. *J. Phys. Chem. Lett.* **2014**, *5*, 1445−1449.
(26) Wang, L.; Liu, B.; Liu, D.; Yao, M.; Hou, Y.; Yu, S.; Cui, T.; Li, D.; Zou, G.; Iwasiewicz, A.; Sundqvist, B. Synthesis of Thin, Rectangular C_{60} Nanorods Using m-Xylene as a Shape Controller. *Adv. Mater.* **2006**, *18*, 1883−1888.
(27) Yuwen, L. H.; Yu, H.; Yang, X. G.; Zhou, J. J.; Zhang, Q.; Zhang, Y. Q.; Luo, Z. M.; Su, S.; Wang, L. H. Rapid Preparation of Single-Layer Transition Metal Dichalcogenide Nanosheets *via* Ultrasonication Enhanced Lithium Intercalation. *Chem. Commun.* **2016**, *52*, 529−532.
(28) Yuwen, L.; Xu, F.; Xue, B.; Luo, Z.; Zhang, Q.; Bao, B.; Su, S.; Weng, L.; Huang, W.; Wang, L. General Synthesis of Noble Metal (Au, Ag, Pd, Pt) Nanocrystal Modified MoS_2 Nanosheets and the Enhanced Catalytic Activity of Pd−MoS_2 for Methanol Oxidation. *Nanoscale* **2014**, *6*, 5762−5769.
(29) Paul, S.; Kanwal, A.; Chhowalla, M. Memory Effect in Thin films of Insulating Polymer and C_{60} Nanocomposites. *Nanotechnology* **2006**, *17*, 145−151.
(30) Yin, Z.; Li, H.; Jiang, L.; Shi, Y.; Sun, Y.; Lu, G.; Zhang, Q.; Chen, X.; Zhang, H. Single-Layer MoS_2 Phototransistors. *ACS Nano* **2012**, *6*, 74−80.
(31) Tongay, S.; Varnoosfaderani, S. S.; Appleton, B. R.; Wu, J.; Hebard, A. F. Magnetic Properties of MoS2: Existence of Ferromagnetism. *Appl. Phys. Lett.* **2012**, *101*, 123105.
(32) Sim, D. M.; Kim, M.; Yim, S.; Choi, M. J.; Choi, J.; Yoo, S.; Jung, Y. S. Controlled Doping of Vacancy- Containing Few-Layer MoS2 *via* Highly Stable Thiol-Based Molecular Chemisorption. *ACS Nano* **2015**, *9* (12), 12115−12123.
(33) Li, H. H.; Wang, Z. X.; Song, C.; Wang, Y.; Lin, Z. M.; Xiao, J. J.; Chen, R. F.; Zheng, C.; Huang, W. Manipulating Charge Transport in a pi-Stacked Polymer through Silicon Incorporation. *J. Mater. Chem. C* **2014**, *2*, 6946−6953.
(34) Son, D. I.; Park, D. H.; Kim, J. B.; Choi, J.; Kim, T. W.; Angadi, B.; Yi, Y.; Choi, W. K. Bistable Organic Memory Device with Gold Nanoparticles Embedded in a Conducting Poly(N-vinylcarbazole) Colloids Hybrid. *J. Phys. Chem. C* **2011**, *115*, 2341−2348.
(35) Jariwala, D.; Howell, S. L.; Chen, K. S.; Kang, J.; Sangwan, V. K.; Filippone, S. A.; Turrisi, R.; Marks, T. J.; Lauhon, L. J.; Hersam, M. C. Hybrid, Gate-tunable, van der Waals *p*−*n* Heterojunctions from Pentacene and MoS_2. *Nano Lett.* **2016**, *16*, 497−503.
(36) Xu, X.; Yin, Z.; Xu, C.; Dai, J.; Hu, J. Resistive Switching Memories in MoS_2 Nanosphere Assemblies. *Appl. Phys. Lett.* **2014**, *104*, 033504.
(37) Bhandavat, R.; David, L.; Singh, G. Synthesis of Surface-Functionalized WS_2 Nanosheets and Performance as Li-Ion Battery Anodes. *J. Phys. Chem. Lett.* **2012**, *3*, 1523−1530.
(38) Zheng, J.; Zhang, H.; Dong, S.; Liu, Y.; Nai, C. T.; Shin, H. S.; Jeong, H. Y.; Liu, B.; Loh, K. P. High Yield Exfoliation of Two-Dimensional Chalcogenides using Sodium Naphthalenide. *Nat. Commun.* **2014**, *5*, 2995.

DOI: 10.1021/acs.chemmater.6b01115
Chem. Mater. 2016, 28, 4300−4306